RSC Advances

PAPER

View Article Online
View Journal | View Issue

Cite this: *RSC Adv.*, 2025, **15**, 44049

Development and optimization of green extraction of naringin in *Citrus grandis* 'Tomentosa' using natural deep eutectic solvents (NADES) and investigation of lung cancer therapeutics mechanisms

Jiaqi Yang,†[a] Guihua Zhang,†[d] Yanghuan Xing,[a] Bixing Gao,[e] Hua Du *[bc] and Guihua Jiang*[a]

Natural bioactive compounds derived from traditional Chinese medicine have garnered widespread research interest. In this study, a green and efficient method for extracting naringin from *Citrus grandis* 'Tomentosa' (CGT) was developed using ultrasonic-assisted extraction (UAE) with the natural deep eutectic solvent (NADES) composed of choline chloride and levulinic acid (ChCl–Le). The extraction was carried out under the conditions of 40% (w/w) water content in NADES, a solid-to-liquid ratio of 1 : 65 (w/v), a temperature of 60 °C, an extraction time of 40 minutes, and an ultrasonic power of 300 W. Despite optimized and practical conditions, a high naringin yield of 4.7% was attained. This yield remains significantly greater than those obtained with methanol (4.1%) or ethanol (4.0%). Furthermore, the CGT extracts were evaluated for lung cancer therapeutics activity, leading to the identification of several key bioactive compounds, including poncirin, isosinensetin, sinensetin, nobiletin, didymin, neohesperidin, and naringenin. These components are known to exert therapeutic effects against lung cancer by targeting CYP17A1, CYP19A1, and AR, as well as by modulating pathways such as EGFR tyrosine kinase inhibitor resistance and prostate cancer. This study successfully establishes an eco-efficient extraction method for naringin and clarifies the multi-target mechanism of action of CGT extracts against lung cancer.

Received 17th October 2025
Accepted 2nd November 2025

DOI: 10.1039/d5ra07966g

rsc.li/rsc-advances

1. Introduction

Citrus grandis 'Tomentosa' is a traditional Chinese medicinal herb widely used to treat respiratory conditions such as cough and bronchitis.[1] Its medicinal properties are largely attributed to flavonoids, among which naringin stands out as the most abundant and representative constituent.[2] Du *et al.*[3] demonstrated that naringin ameliorates the immunosuppressive tumor microenvironment by downregulating transforming growth factor-β1 (TGF-β1) and reducing regulatory T cells. Park *et al.*[4] further reported that naringin induces reactive oxygen species (ROS) production and activates the MAPK pathway, thereby exerting anti-cancer effects in choriocarcinoma cells. These findings collectively highlight the substantial pharmaceutical potential of naringin.

Consequently, developing efficient and sustainable methods for naringin extraction from CGT is crucial. Conventional extraction techniques rely heavily on organic solvents such as methanol and ethanol, often combined with heat-assisted or Soxhlet extraction.[5] These approaches, however, are limited by the inherently low concentration of naringin in CGT, as well as its poor solubility in common solvents, resulting in low extraction efficiency.[6] Additionally, the high toxicity, volatility, and poor biodegradability of these solvents pose significant environmental and safety risks.[7]

In recent years, alternative extraction techniques have gained attention, including ultrasonic-assisted extraction and subcritical fluid extraction.[8,9] Among these, UAE is recognized for its high efficiency, short processing time, and low operating temperature, making it highly attractive for laboratory-scale use.[10] Nevertheless, its industrial application is still constrained by challenges such as noise pollution and a limited effective extraction area due to acoustic attenuation. Moreover, while methods like UAE can enhance extraction performance, they often continue to depend on conventional solvents,

[a]*College of Pharmacy, Chengdu University of TCM, Sichuan 611137, China. E-mail: jiangguihua@cdutcm.edu.cn*

[b]*Chongqing Institute of Medicinal Plant Cultivation, Chongqing 408400, China. E-mail: 1432145369@qq.com*

[c]*Department of Preparation Center, Chongqing Hospital of Traditional Chinese Medicine, Chongqing 400014, China*

[d]*Department of Pharmacy, Yunnan Provincial Hospital of Traditional Chinese Medicine, Yunnan, 650021, China*

[e]*Sichuan Institute for Drug Control, Key Laboratory of Quality Evaluation of Chinese Patent Medicines, Sichuan 611700, China*

† These authors contributed equally to this work and they are co-first authors.

meaning the fundamental issue of environmental sustainability remains largely unresolved.[11]

To address the core issue of environmental sustainability, attention has turned to green solvents such as Natural Deep Eutectic Solvents (NADES). NADES are formed by mixing hydrogen bond acceptors (HBA) and hydrogen bond donors (HBD) in specific ratios.[12] Through intermolecular hydrogen bonding, these components create stable liquid mixtures with significantly depressed melting points and unique solubilizing properties.[13] In recent years, NADES have attracted increasing interest as sustainable media for extracting bioactive compounds. Compared to conventional organic solvents, they offer advantages such as low cost, high biodegradability, ease of preparation, and low toxicity, making them highly suitable for extracting bioactive constituents from various plant materials.[14]

Building on these advantages, the integration of NADES with ultrasonic-assisted extraction (NADES-UAE) has emerged as a particularly promising strategy. For instance, Liu *et al.*[15] developed a combined NADES-UAE and anti-solvent purification method for the efficient extraction and refinement of scutellarin from *Erigerontis Herba*. Similarly, Wu *et al.*[16] successfully applied a NADES-UAE system to extract anthraquinones from *Rheum palmatum* L., reporting that an optimized solvent composed of lactic acid, glucose, and water achieved high extraction efficiency. These studies underscore that NADES, when synergistically combined with ultrasonication, not only enhance extraction performance but also offer an eco-friendly platform for recovering active components from traditional Chinese medicines.[17–19]

Given the promising synergy between NADES and UAE demonstrated in previous studies,[20] their application for naringin extraction from CGT remains underexplored. Moreover, although naringin is known to possess anticancer activity, its specific mechanisms of action against lung cancer require deeper elucidation. The present study is designed with the following objectives: (1) to establish an efficient and environmentally friendly NADES-UAE system for extracting naringin from CGT by screening 19 NADES formulations; (2) to optimize the key extraction parameters using a combination of single-factor experiments and response surface methodology (RSM); and (3) to preliminarily investigate the anti-lung cancer mechanisms of the extracted naringin using network pharmacology and molecular docking, thereby providing a theoretical basis for its future application in functional foods or therapeutics.

2. Materials and methods

2.1 Material and chemical reagent

2.1.1 Materials needed for naringin extraction. The dried peel of CGT was purchased from Sichuan Hongkangyuan Pharmaceutical Co., Ltd Professor Jiang Guihua of Chengdu University of Traditional Chinese Medicine identified it as immature or nearly mature dry outer peel of *Citrus grandis 'Tomentosa'* or *Citrus grandis 'tomentosa' of* Rutaceae. Choline chloride (≥98%), L-proline (≥99%), betaine (≥9%), lactic acid (85–90%), acetic acid (HPLC grade, ≥99.8%), tartaric acid (≥99%), ethylene glycol (≥98%), 1,4-butanediol (≥99%), isosorbide (>98%), citric acid (≥99.5%), urea (≥99%), DL-malic acid (>99%), glycerol (≥99%), and arabitol (≥98%, analytical grade) were purchased from Shanghai Aladdin Biochemical Technology Co., Ltd Methanol (≥99.9%, HPLC grade) was obtained from Shanghai Macklin Biochemical Co., Ltd Naringin standard (≥98%, HPLC grade) was purchased from Chengdu Desite Biotechnology Co., Ltd The chemicals of different purities were directly used in the experiments without further purification.

2.1.2 Instrumentation and equipments. SCIEX X500R QTOF high-resolution mass spectrometer (SCIEX, USA; resolution 40 000 FWHM), JA3003J electronic analytical balance (SHUNYU, China; precision 0.001 g), AXLM1820-2 ultrapure water system (ASURA, China; 18.2 MΩ cm), AS10200AT ultrasonic cleaner (Autoscience, China; 200 W, 40 kHz), SL-1000 high-speed grinder (Songqing, China; 25 000 rpm).

All instruments were calibrated according to ISO/IEC 17025 standards prior to use.

2.2 Preparation of NADES

NADES were prepared by mixing hydrogen bond acceptors (HBAs) and donors (HBDs) at predetermined molar ratios. Three HBAs (proline, betaine, and choline chloride) were weighed into separate 50 mL glass flasks. Corresponding HBDs were then added to their respective flasks. Because the viscosity of different NADES varies greatly, 20% water is added to them to ensure the same water content.[21] The mixtures were homogenized using a magnetic stirrer in an oil bath with constant stirring at 500 rpm for 30 min maintained at 80 °C until forming homogeneous liquids. The compositions of NADES solvents prepared with different HBAs are detailed in Table S1–S3.

2.3 Extraction of naringin

For preliminary NADES screening, 0.10 g of CGT powder was weighed into a 25 mL glass-stoppered conical flask. Subsequently, 6.0 g of pre-synthesized NADES was added (solid-to-liquid ratio 1 : 60 w/v). Parallel extractions using methanol and deionized water were performed under identical conditions: ultrasonication at 40 kHz and 300 W in a temperature-controlled bath maintained at 30 °C for 30 min. For preliminary screening, fixed power at 300 W was used. In subsequent single-factor tests, power was varied. After extraction, solutions were quantitatively transferred to 25 mL volumetric flasks, diluted with deionized water, and filtered (0.22 μm) prior to HPLC analysis. All extractions were performed in triplicate. The result of the extraction rate is presented as a percentage (%). The extraction yield (Y) was calculated as:

$$Y = \frac{c \times v}{m}$$

where c (mg mL^{-1}) represents naringin concentration, v (mL) denotes the final solution volume, and m (g) corresponds to the initial sample mass.

A single-factor test was used to examine how the parameters of the extraction process affected the amount of naringin. Nineteen distinct deep eutectic solvents, various molar ratios of

HBA to HBD (1 : 1, 1 : 2, 1 : 3, 1 : 4, 1 : 5), water contents (10%, 20%, 30%, 40%, 50%, 60%), extraction temperatures (30, 40, 50, 60, 70 °C), extraction times (10, 20, 30, 40, 50, 60 min), solid–liquid ratios (1 : 30, 1 : 40, 1 : 50, 1 : 60, 1 : 70), and power (50, 100, 150, 200, 250, 300 W) were among the various conditions used in the experiments.

2.4 HPLC analysis conditions

High-performance liquid chromatography (HPLC) was employed for the quantitative measurement of naringin. The chromatographic parameters are as follows: Phenomenex C18 (250 mm × 4.6 mm, 5 μm), Column temperature: 30 °C, Sample volume: 10 μL, Flow rate: 1.0 mL min^{-1}, Detection wavelength: 283 nm, The gradient elution protocols for the mobile phases 0.1% phosphoric acid-water (a) and acetonitrile (b) are detailed as follows: 0–2 min 90% A, 2–5 min 90% to 85% A, 5–10 min 85% to 82% A, 10–32 min 82% to 80% A, 32–45 min 80% → 60% A, 45–60 min 60% → 40% A, 60–60 min 40% → 0 A.

2.5 Optimization of the extraction conditions using RSM

The extraction techniques were optimized using a Box–Behnken design (BBD). Based on the optimization results from single-factor experiments, three key parameters influencing naringin yield were selected: extraction time (X_1), temperature (X_2), and solid–liquid ratio (X_3). These factors were investigated at three coded levels (−1, 0, +1). A three-factor, three-level BBD experiment was then conducted, with naringin yield (Y) as the response variable. The experimental factors and their levels are summarized in Table S4. Analyzed using Design Expert 13 to generate the response surface model, a total of 15 sets of tests were created in order to optimize the three-factor, three-level response surface test. A second-order polynomial equation obtained by multiple regression analysis is as follows:

$$Y = \beta_0 + \sum_{i=1}^{k} \beta_i X_i + \sum_{i=1}^{k} \beta_{ii} X_i^2 + \sum_{i=1, i<j}^{k} \sum_{j=2}^{k} \beta_{ij} X_i X_j$$

where X_i and X_j represent independent encoded variables of Y, Y represents the response variable, β_0 is a constant, β_i, β_{ii}, and β_{ij} are linear constants, quadratic constants, and interaction constants, respectively, all of which are regression coefficients, K represents the number of variables.

The responses were determined under the optimum extraction conditions. Finally, the experimental data were compared with the predicted values using the standard errors to validate the model. The single factor analysis of variance (ANOVA) was used to compare the extraction rate of naringin.

2.6 Reusability of NADES

A series of recycling experiments were performed to assess the cost-effectiveness and reusability of the natural deep eutectic solvent ChCl–Le for naringin extraction. The extraction was carried out under the previously optimized conditions. Following extraction and filtration, the ChCl–Le solvent was directly reused to process a subsequent batch of fresh raw material. This process was repeated multiple times. The naringin concentration in the solvent was analytically monitored after each cycle to quantify its gradual accumulation.

2.6.1 Scanning electron microscopy. To evaluate the effects of different solvents (ChCl–Le, methanol, and water) on the surface structure of the plant cell wall after the ultrasonic extraction of CGT, the morphologies of the original CGT powder and of the thoroughly washed and dried solid residues from each extraction process were examined using a Thermo Scientific™ APREO scanning electron microscope (SEM). The key sample preparation steps were as follows: First, each solid residue was washed extensively with its corresponding pure solvent (*i.e.*, ChCl–Le extraction residue with ChCl–Le, methanol extraction residue with methanol, and water extraction residue with water) to remove residual solvent components as completely as possible. For the residue from ChCl–Le extraction, an additional washing step with anhydrous ethanol was conducted to ensure complete removal of any residual ChCl–Le. Subsequently, the samples were dried by either low-temperature vacuum drying (at 40 °C) or, preferably, freeze-drying. This careful drying procedure was critical to minimize drying stress, thereby preserving the native sample morphology and preventing structural distortion that could arise from the volatilization of residual solvent or from adhesive interactions under the high-vacuum environment of the SEM. After washing and drying, the samples were mounted on aluminum stubs and sputter-coated with a thin conductive gold layer prior to SEM imaging.

2.7 Statistical analysis

All the experiments were carried out in triplicates. SPSS 30.0.0 statistical software (IBM, USA) was used for standard deviation calculations, pictures were done using GraphPad Prism 8.0.2 software.

2.8 LC-MS structural analysis

Chromatographic conditions were as follows: A 2.1 × 100 mm C18 reversed-phase column packed with 1.7 μm particles was used. The mobile phase consisted of (A) 0.1% aqueous formic acid and (B) acetonitrile. The gradient elution program was set as: 0–5 min, 10% B (90% A), 5–15 min, linear gradient from 10% to 50% B, 15–30 min, linear gradient from 50% to 100% B, 30–40 min, isocratic at 100% B, 40–40.1 min, linear gradient back to 10% B, 40.1–45 min, isocratic at 10% B for column re-equilibration. The flow rate was 0.5 mL min^{-1}, the column temperature was maintained at 40 °C, and the injection volume was 3 μL.

Mass spectrometry conditions were as follows: Electrospray ionization (ESI) source was operated in both positive and negative ion modes. The spray voltage was set to +5500 V for positive mode and −4500 V for negative mode. Ion source parameters included: a desolvation temperature of 550 °C, sheath gas pressure, 50 arbitrary units, auxiliary gas pressure, 50 arbitrary units (or specify if different). The TOF mass analyzer acquired data over the range of m/z 50 to 1500 Da.

Spectral data processing was performed using Compound Discoverer 3.1, with compound annotation against HMDB,

PubChem, and custom databases. Identification criteria included retention time consistency, accurate mass measurement, and MS/MS spectral matching with a similarity threshold of ≥80%.

2.9 Network pharmacology and molecular docking

2.9.1 Procurement of active constituents and therapeutic goals of CGT. The active ingredients of the traditional Chinese medicine Huajuhong (Latin name: *Citrus grandis* 'Tomentosa') were retrieved from the Traditional Chinese Medicine Systems Pharmacology Database and Analysis Platform (TCMSP). Potential bioactive constituents were selected based on two key pharmacokinetic parameters: oral bioavailability (OB) ≥ 30% and drug-likeness (DL) ≥ 0.18. Subsequently, Lipinski's Rule of Five (Ro5) was applied for further filtering, with thresholds set as molecular weight (MW) ≤ 500, MLogP ≤ 5, number of hydrogen bond donors (nHBD) ≤ 5, and number of hydrogen bond acceptors (nHBA) ≤ 10.

The chemical structures (*e.g.*, in SMILES format) of the resulting compounds were obtained from the PubChem database. These structures were then submitted to the SwissTargetPrediction database to forecast their putative targets. Finally, duplicate target entries were removed to generate a unique set of protein targets for the active components of Huajuhong.

2.9.2 The putative targets of lung cancer collection. Using the search term "lung cancer," the possible targets were found in the OMIM database (**https://www.omim.org/**) and GeneCards database (**https://www.genecards.org/**), with the species restricted to "*Homo sapiens*." To obtain the potential targets, the duplicate targets were then eliminated.

2.9.3 Acquisition of intersection target of traditional Chinese medicine and disease. First, the official gene symbols for the targets associated with both lung cancer and the active components of Huajuhong decoction were standardized using the UniProt database (**https://www.uniprot.org/**). Then, to identify the intersection targets and ultimately determine the putative therapeutic targets for lung cancer treatment, a Venn diagram was generated to visualize the overlap between the active component targets and the lung cancer disease targets.

2.9.4 Protein–protein interaction (PPI) network development. The intersection targets were imported into the STRING database (**https://string-db.org/**), with the species defined as "human" and the minimum interaction confidence score set to 0.4. This was done to retrieve protein–protein interaction (PPI) information and generate the PPI network. To further screen for the most likely core targets of Huajuhong decoction acting on lung cancer, the PPI data obtained from STRING was imported into Cytoscape 3.7.2. The PPI network was then visualized and analyzed within Cytoscape to identify key targets.

2.9.5 Pathway enrichment performance. The intersection targets were imported into the DAVID database (**https://david.ncifcrf.gov/**) for functional annotation and pathway enrichment analysis. Gene Ontology (GO) and Kyoto Encyclopedia of Genes and Genomes (KEGG) pathway enrichment analyses were performed, with the identifier type set to "OFFICIAL_GENE_SYMBOL" (or "Gene List"), and the species limited to "*Homo sapiens*". The top 20 significantly enriched GO terms and KEGG pathways were visualized. Bar plots for the top 20 GO terms were generated using GraphPad Prism, while the top 20 KEGG pathway enrichment results were visualized using the ggplot2 package in R.

2.9.6 Molecular docking. The initial two-dimensional (2D) structures of the top seven small-molecule ligands, selected based on degree centrality, were retrieved from PubChem. These structures were then imported into ChemDraw3D for geometry optimization. Using the MM2 force field *via* the Calculations menu, energy minimization was performed to generate their stable three-dimensional (3D) conformations. The optimized 3D structures were subsequently exported for docking studies. Concurrently, the ten protein receptors with the highest degree centrality were obtained from the Protein Data Bank (PDB). Using PyMOL (v2.5.2), crystallographic water molecules and any co-crystallized ligands were removed from these protein structures to prepare them for docking. Molecular docking simulations were carried out using AutoDock Vina. The resulting protein-ligand complexes were then visualized and analyzed for interaction modes using both PyMOL (v2.5.2) and Discovery Studio (v2019).

3. Results and discussion

3.1 Extraction of naringin with different solvents

As shown in Fig. 1, 21 different solvents were evaluated under standardized conditions (30 °C, 300 W ultrasonic power, 30 minutes). To mitigate the high viscosity of NADES which impedes mass transfer, all NADES formulations were pre-diluted with 20% (v/v) water. Notably, all NADES systems outperformed conventional solvents (methanol and ethanol) in extracting naringin. Among them, NADES-9, composed of choline chloride and levulinic acid (ChCl–Le), achieved the highest extraction yield (4.3%), followed by NADES-16 and NADES-15 (both 4.2%). In comparison, NADES-5 (3.95%) and NADES-12 (3.90%) showed relatively lower efficiency. The superior performance of NADES-9 (ChCl–Le) can be attributed to a synergistic mechanism: firstly, they disrupt the plant cell wall, enhancing solvent accessibility; secondly, their functional groups engage in favorable molecular interactions, primarily hydrogen bonding with naringin.[22,23] This combination of improved mass transfer and enhanced solubility underpins the high extraction efficiency. Consequently, ChCl–Le was selected as the optimal solvent for subsequent optimization and mechanistic studies.

3.2 Selection of initial extraction method and conditions

The molar ratio of hydrogen bond acceptor (HBA, ChCl) to hydrogen bond donor (HBD, Le) was identified as a critical parameter governing naringin extraction efficiency, as delineated in Fig. 2A Under the initial conditions (20% water content, 30 °C, 300 W ultrasonic power, 30 min extraction time, with triplicate extractions). That is, unoptimized conditions, the maximum yield of 4.3% was achieved at a ChCl : Le molar ratio of 1 : 2. This optimum represents a balance where the NADES

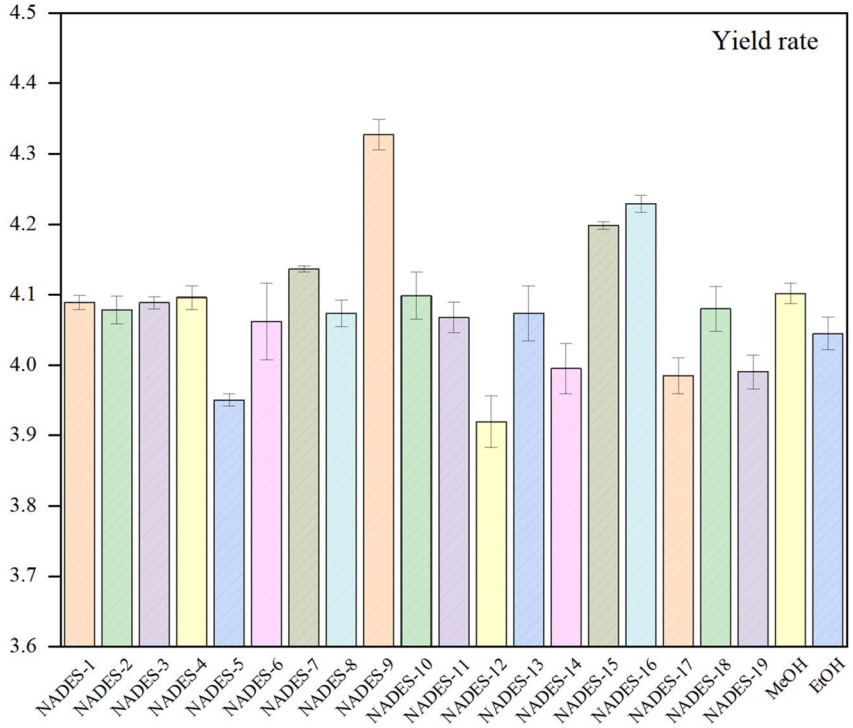

Fig. 1 Effects of NADESs and conventional solvents on the yield of naringin.

possesses an ideal physicochemical profile for both disrupting the plant matrix and solubilizing naringin. Deviating from this ratio, particularly towards an HBD-rich system (*e.g.*, 1 : 5), resulted in diminished efficiency. This decline is likely due to the NADES system approximating the properties of pure levulinic acid, which exhibits higher viscosity and a less effective hydrogen-bonding network for naringin solubilization. Therefore, the HBA/HBD molar ratio is paramount, as it extends

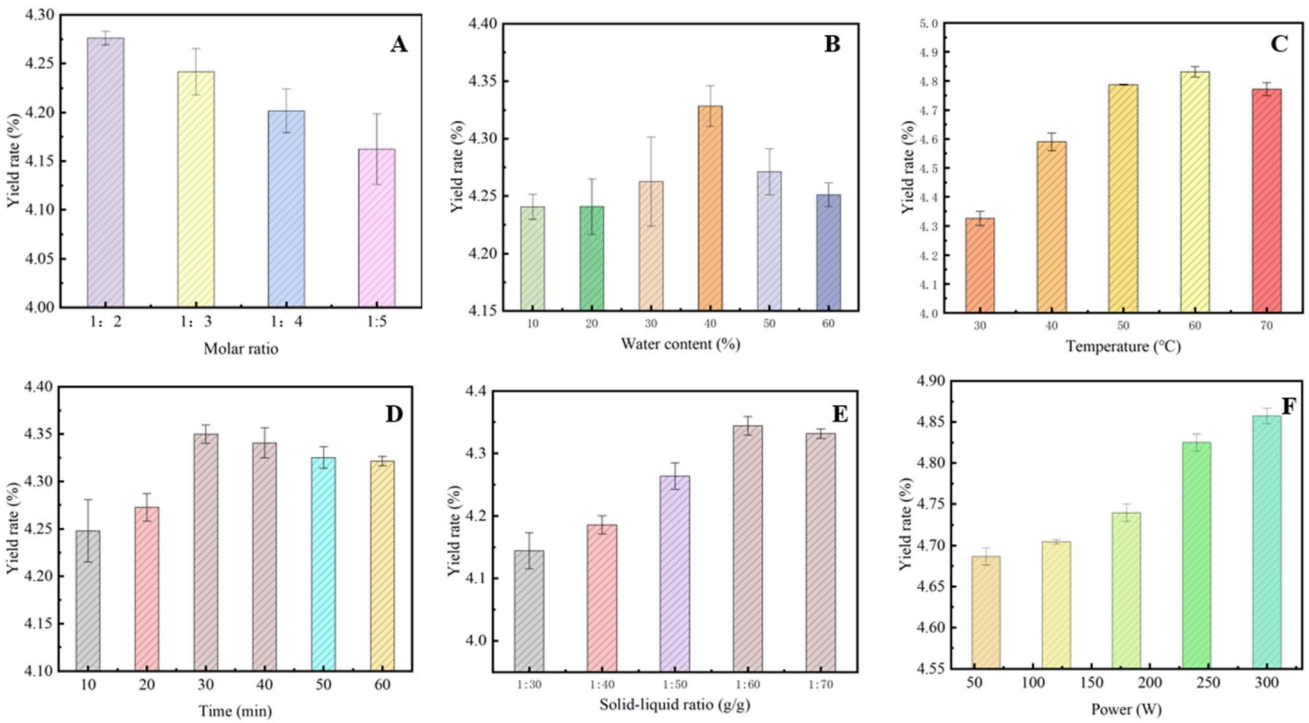

Fig. 2 Contents of extraction of naringin with ChCl–Le (1 : 2) from CGE. (A) Effect of the molar ratio of ChCl–Le, (B) water content in NADES/water solution, (C) extraction temperature, (D) extraction time, (E) solid/liquid ratios (F) power on extracted amounts of naringin from CGE using UAE. Error bars indicate the relative standard deviation ($n = 3$).

beyond the mere formation of a NADES to critically dictate the solvent's intermolecular interactions and viscosity, which in turn govern extraction performance.[24]

As is illustrated in Fig. 2B, the effect of water content in the NADES/water mixture on naringin extraction efficiency was investigated. The experiments were conducted using ChCl–Le (1 : 2) as the extraction solvent under fixed conditions: an ultrasonic power of 300 W, a temperature of 30 °C, and an extraction time of 30 min. All experiments were performed in triplicate, and the average values are reported. The highest naringin extraction yield was 4.3%, achieved at a water content of 40%. Beyond this optimum, further increases in water content from 40% to 60% resulted in a gradual decline in the extraction yield.

This trend can be explained by the effect of water content on the viscosity and mass transfer properties of the solvent.[25] At water levels below 40%, the reduced viscosity of the NADES enhances its penetration into the plant matrix and improves mass transfer, facilitating the diffusion of naringin from the plant cells into the solvent. Conversely, when the water content exceeds 40%, excessive water molecules disrupt the hydrogen-bonding network within the NADES. This structural weakening reduces the solvent's interaction with naringin, resulting in decreased extraction performance.[26]

As shown in Fig. 2C and D, the effects of ultrasonic temperature and extraction time on naringin yield were investigated. The naringin yield increased significantly with temperature up to 60 °C, reaching a maximum of 4.8%. Beyond this optimum temperature, a further increase led to a noticeable decline in yield. This trend can be explained by the following mechanisms: at temperatures below 60 °C, increasing temperature reduces the viscosity of the NADES system and enhances the thermal motion of both naringin molecules and the solvent.[27] The penetration of the solvent into the plant matrix is improved, facilitating the dissolution and diffusion of naringin and resulting in increased extraction efficiency. Conversely, when the temperature exceeds 60 °C, the excessive thermal energy disrupts the intermolecular interactions within the NADES—particularly the hydrogen bonding network—compromising its stability and extraction capability.[28] Moreover, elevated temperatures may cause partial degradation of naringin, resulting in reduced overall yield.

When the extraction duration was shorter than 30 minutes, the naringin yield increased steadily, attaining a maximum of 4.3% at exactly 30 minutes under these conditions. However, extending the extraction time beyond 30 minutes—up to 60 minutes—resulted in a consistent decline in naringin yield. This pattern can be attributed to the following mechanisms: within the first 30 minutes, the combined effects of ultrasonic cavitation, mechanical energy, and thermal energy promote the disruption of plant cell walls, facilitating the rapid release and dissolution of naringin.[29] The polarity affinity of NADES further enhances extraction efficiency during this period, contributing to higher naringin yields. Beyond 30 minutes, prolonged exposure to ultrasonic and thermal energy may lead to the degradation of naringin due to increased energy input and elevated system temperatures.[30] Additionally, extended extraction durations can destabilize the interaction between NADES and the CGT matrix, potentially altering the structural integrity of naringin and reducing overall extraction yield.[6,31]

The solid–liquid ratio significantly influenced naringin yield, demonstrating a parabolic relationship, as shown in Fig. 2E The yield increased with increasing solvent volume, reaching an optimum value of 4.3% at a ratio of 1 : 60 (g mL^{-1}). This initial improvement can be attributed to enhanced mass transfer, as a sufficient solvent volume ensures complete contact and efficient penetration into the plant matrix. However, beyond the optimal ratio, a decrease in yield was observed. This decline may be explained by two factors: (1) a reduction in ultrasonic energy density per unit volume, which weakens cavitation-induced cell wall disruption; and (2) co-dissolution of competing impurities,

Table 1 Experimental design and yield of naringin

Experiment number	Extraction time (min)	Extraction temperature (°C)	Solid–liquid ratio (g g^{-1})	Naringin yield (%)
1	30	55	50	4.542
2	20	55	60	4.672
3	40	55	60	4.598
4	30	55	70	4.660
5	20	60	50	4.815
6	40	60	50	4.716
7	30	60	60	4.915
8	30	60	60	4.926
9	30	60	60	4.970
10	20	60	70	4.881
11	40	60	70	4.941
12	30	65	50	4.864
13	20	65	60	4.884
14	40	65	60	4.775
15	30	65	70	4.784

Table 2 Results of analysis of variance[a]

Variance source	Sum of squares	Degrees of freedom	Variance	*F* value	*P* value
Regression model	0.2342	9	0.0260	10.25	0.0098
A	0.0062	1	0.0062	2.43	0.1800
B	0.0872	1	0.0872	34.33	0.0021
C	0.0135	1	0.0135	5.33	0.0690
AB	0.0003	1	0.0003	0.1206	0.7425
AC	0.0063	1	0.0063	2.49	0.1754
BC	0.0098	1	0.0098	3.86	0.1066
A^2	0.0058	1	0.0058	2.27	0.1923
B^2	0.1008	1	0.1008	39.72	0.0015
C^2	0.0130	1	0.0130	5.11	0.0734
Residual items	0.0127	5	0.0025		
Omission item	0.0110	3	0.0037	4.33	0.1933
Pure error	0.0017	2	0.0008		
Amount to	0.2469	14			

[a] Note: $P < 0.01$ indicates a highly significant difference; $P < 0.05$ indicates a significant difference.

complicating the extraction environment and potentially interfering with yield quantification.

Ultrasonic power was also identified as a critical parameter affecting naringin extraction (Fig. 2F). Extraction efficiency increased with rising power up to 300 W, which can be ascribed to intensified cavitation effects promoting more effective cell wall breakdown and solvent convection.[32] Although higher power levels could theoretically enhance cavitation further, 300 W was established as the optimal condition. Beyond this point, the marginal improvement in yield would not justify the substantially increased energy consumption and operational costs.

3.3 Optimizing extraction conditions through BBD-RSM

To ensure operational stability and robust statistical analysis, 15 randomized experimental runs incorporating three central points were conducted using a Box-Behnken design (BBD). Key extraction parameters—previously identified through single-factor experiments—were systematically optimized by selecting three independent variables known to exert significant main effects: extraction time (X_1, 30–50 min), temperature (X_2, 50–70 °C), and liquid-to-solid ratio (X_3, 1 : 50–1:70 g mL^{-1}). The functional relationship between these coded variables and naringin

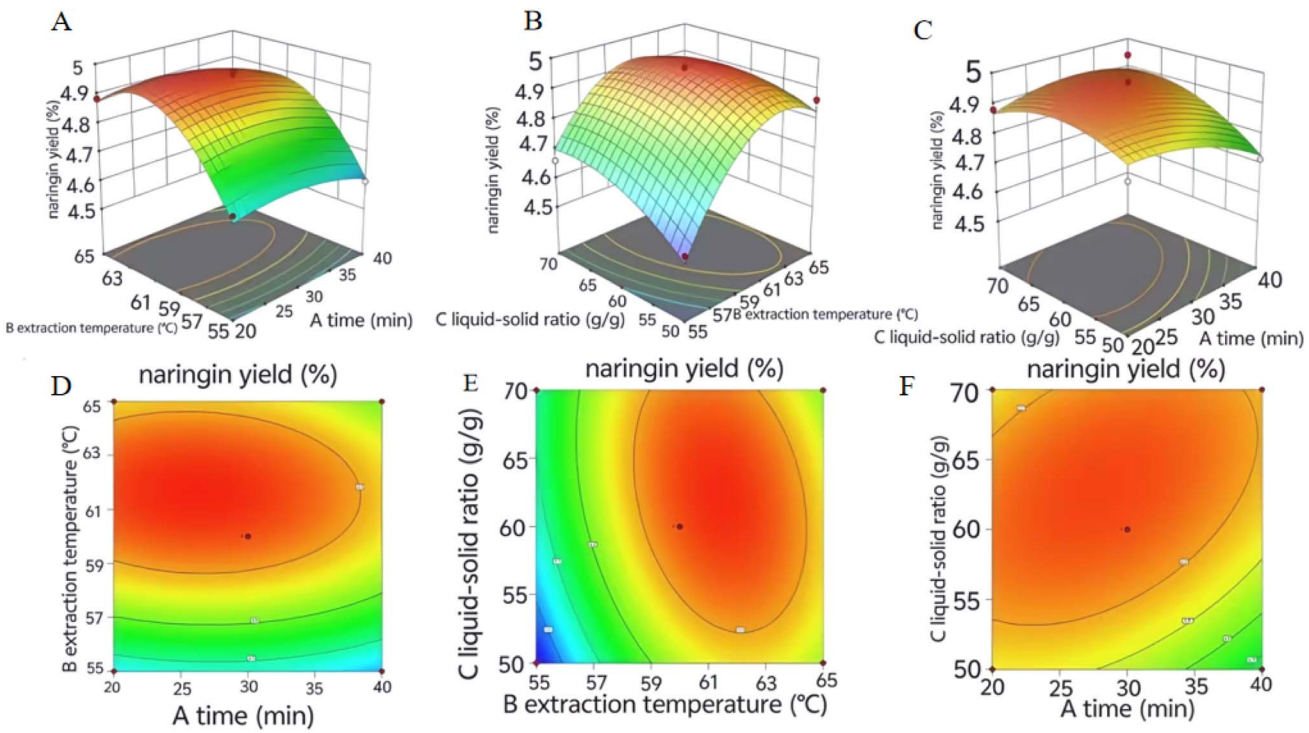

Fig. 3 The three-dimensional (3D) plots and two-dimensional (2D) as a function of extraction time, solid–liquid ratio, and water content in extraction temperature.

yield (Y, %) was quantitatively modeled using a second-order polynomial equation:

$$Y = 4.94 - 0.0278\ A + 0.1044\ B + 0.0411\ C - 0.0087\ AB + 0.0397\ AC - 0.0495\ BC - 0.0395\ A^2 - 0.1652\ B^2 - 0.0593\ C^2.$$

Here, A, B, and C represent extraction temperature, time, and liquid-to-solid ratio, respectively. Analysis of variance (ANOVA) was employed to evaluate the reliability of the regression model, with P-values used to assess the significance of each term. The model was found to be highly significant ($P < 0.01$), and a non-significant lack-of-fit term ($P > 0.05$) confirmed its validity and adequacy. The high coefficient of determination ($R^2 = 0.9486$) and adjusted R^2 (0.8560) indicated a strong correlation between predicted and experimental values, affirming the model's predictive capability for naringin extraction from CGT (Tables 1 and 2).

Response surface methodology (RSM), as visualized by the 2D contour and 3D surface plots (Fig. 3A–F), revealed significant interactive effects among the process variables. Using numerical optimization, the ideal extraction parameters were determined to be 40 min, 60 °C, and a liquid-to-solid ratio of 1 : 65 g mL^{-1}, with the water content in the natural deep eutectic solvent (NADES) fixed at 40%. Under these optimized conditions, the model predicted a naringin yield of 4.9%. Experimental validation yielded 4.7%, which confirms the model's reliability and practical applicability.

The optimal temperature of 60 °C can be attributed to its effect on solvent viscosity and mass-transfer kinetics. An increase in temperature reduces the viscosity of the NADES, thereby enhancing its diffusivity and improving penetration into the plant matrix.[33] This decrease in viscosity consequently raises the mass transfer coefficient, facilitating more efficient solvent ingress and promoting naringin dissolution. Additionally, elevated temperatures strengthen hydrogen-bonding interactions between the hydroxyl groups of naringin and the NADES components, which further shifts the solubility equilibrium toward enhanced extraction efficiency.

Table 3 Active ingredients of CGT

Mol ID	Molecule name	OB (%)	DL
MOL010267	Lycopene	32.57	0.51
MOL013276	Poncirin	36.55	0.74
MOL013277	Isosinensetin	51.15	0.44
MOL013279	5,7,4′-Trimethylapigenin	39.83	0.3
MOL001798	Neohesperidin	71.17	0.27
MOL001803	Sinensetin	50.56	0.45
MOL000358	Beta-sitosterol	36.91	0.75
MOL004328	Naringenin	59.29	0.21
MOL005828	Nobiletin	61.67	0.52
MOL005849	Didymin	38.55	0.24

The extraction time of 39 min represents a balance between extraction kinetics and compound stability. Prolonged exposure to elevated temperature and ultrasonic energy increases the risk of thermal or oxidative degradation of flavonoids, which are structurally sensitive to harsh extraction conditions.[34] Thus, the identified duration allows near-complete extraction while minimizing degradation. Concurrently applied ultrasonication at 300 W enhances extraction efficiency through cavitation effects. These effects generate micro-jets and intense shear forces that disrupt plant cell walls, reduce particle size, and diminish diffusion barriers—thereby significantly accelerating the release of naringin into the solvent.

In summary, the Box–Behnken Design (BBD) model not only identifies optimal extraction conditions but also aligns closely with fundamental physicochemical principles. The results underscore the importance of the interplay between solubility enhancement, diffusive transport, and molecular stability in the efficient extraction of flavonoids such as naringin.

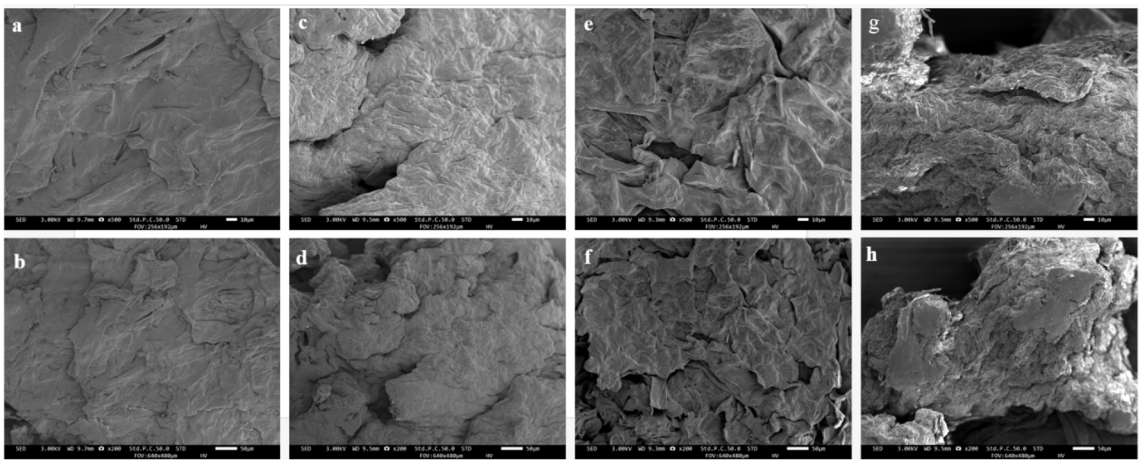

Fig. 4 SEM images of CGT before extraction and after extraction (the extraction conditions were: L/S = 1 : 66, 20% V/V, water 61 °C, 39 min). a and b Are unprocessed medicinal powders. c and d Are extracted after water extraction. e and f Are extracted after methanol extraction. g and h Are extracted from Choline chloride-levulinic acid.

Table 4 Binding energies of key active compounds with core targets

Serial number	Target spot	PDB ID	Ingredient	Binding energy (kcal mol^{-1})
1	CCND1	6PBE	5,7,4′-Trimethylapigenin	−7.0
2			Didymin	−8.2
3			Sosinensetin	−6.8
4			Nobiletin	−6.4
5			Sinensetin	−7.1
6			Naringenin	−7.1
7			Neohesperidin	−8.1
8	PARP1	7AAC	5,7,4′-Trimethylapigenin	−6.4
9			Didymin	−6.7
10			Sosinensetin	−6.1
11			Nobiletin	−6.4
12			Sinensetin	−6.1
13			Naringenin	−5.9
14			Neohesperidin	−7.1
15	AKT1	7MYX	5,7,4′-Trimethylapigenin	−6.5
16			Didymin	−7.5
17			Sosinensetin	−6.1
18			Nobiletin	−6.0
19			Sinensetin	−6.8
20			Naringenin	−6.3
21			Neohesperidin	−6.5
22	ESR1	7RS8	5,7,4′-Trimethylapigenin	−7.7
23			Didymin	−9.1
24			Sosinensetin	−7.1
25			Nobiletin	−6.8
26			Sinensetin	−7.2
27			Naringenin	−8.3
28			neohesperidin_qt	−8.5
29	EGFR	8A2D	5,7,4′-Trimethylapigenin	−8.2
30			Didymin	−9.4
31			Sosinensetin	−7.8
32			Nobiletin	−8.1
33			Sinensetin	−8.3
34			Naringenin	−8.1
35			Neohesperidin	−7.8
36	BCL2	8HOG	5,7,4′-Trimethylapigenin	−6.8
37			Didymin	−8.6
38			Sosinensetin	−6.6
39			Nobiletin	−6.8
40			Sinensetin	−6.5
41			Naringenin	−7.4
42			Neohesperidin	−7.8
43	MMP9	8K5Y	5,7,4′-Trimethylapigenin	−9.4
44			Didymin	−9.5
45			Sosinensetin	−7.6
46			Nobiletin	−8.2
47			Sinensetin	−8.2
48			Naringenin	−7.9
49			neohesperidin_qt	−9.5
50	SRC	8VCG	5,7,4′-Trimethylapigenin	−7.1
51			Didymin	−10.9
52			Sosinensetin	−8.8
53			Nobiletin	−6.8
54			Sinensetin	−8.8
55			Naringenin	−8.9
56			neohesperidin_qt	−8.0
57	MTOR	8XI9	5,7,4′-Trimethylapigenin	−7.2
58			Didymin	−8.9
59			Sosinensetin	−7.1
60			Nobiletin	−6.7
61			Sinensetin	−7.2
62			Naringenin	−7.5
63			Neohesperidin	−7.8

3.4 Morphological characterization of CGT residues

Fig. 4 presents scanning electron microscopy (SEM) images of untreated CGT powder and samples extracted with water, methanol, and the optimized NADES (ChCl–Le, 1 : 2). The untreated powder exhibits a smooth, intact surface, indicating preserved cellular structure. In contrast, ultrasonic extraction induced varying microstructural changes: water caused mild shrinkage while maintaining surface continuity, consistent with its moderate polarity; methanol led to more obvious wrinkling and fragmentation of surface fibers, reflecting its stronger solvent action. The most severe disruption occurred with NADES, which resulted in extensive fiber disintegration, cellular rupture, and debris formation. This aligns with reports that certain NADES effectively disrupt cell walls, enhancing the release of metabolites such as naringin.[35–37]

3.5 Reusability assessment of NADES

The reusability of the NADES system was evaluated, and the results are presented in Fig. S1. The cumulative naringin yield from the same batch of CGT material reached 4.8%, 9.4%, 13.9%, 18.6%, and 22.8% over one to five extraction cycles using recycled NADES, respectively. The yield increased steadily with each cycle, and the incremental gain remained stable and consistent with that of the first extraction. These findings confirm that ChCl–Le can be effectively reused for at least five consecutive extraction cycles without significant loss of efficiency, demonstrating its potential for sustainable and economical extraction processes.

3.6 Study on anticancer mechanism

Lung cancer is broadly categorized into non-small cell lung cancer (NSCLC) and small cell lung cancer (SCLC). SCLC

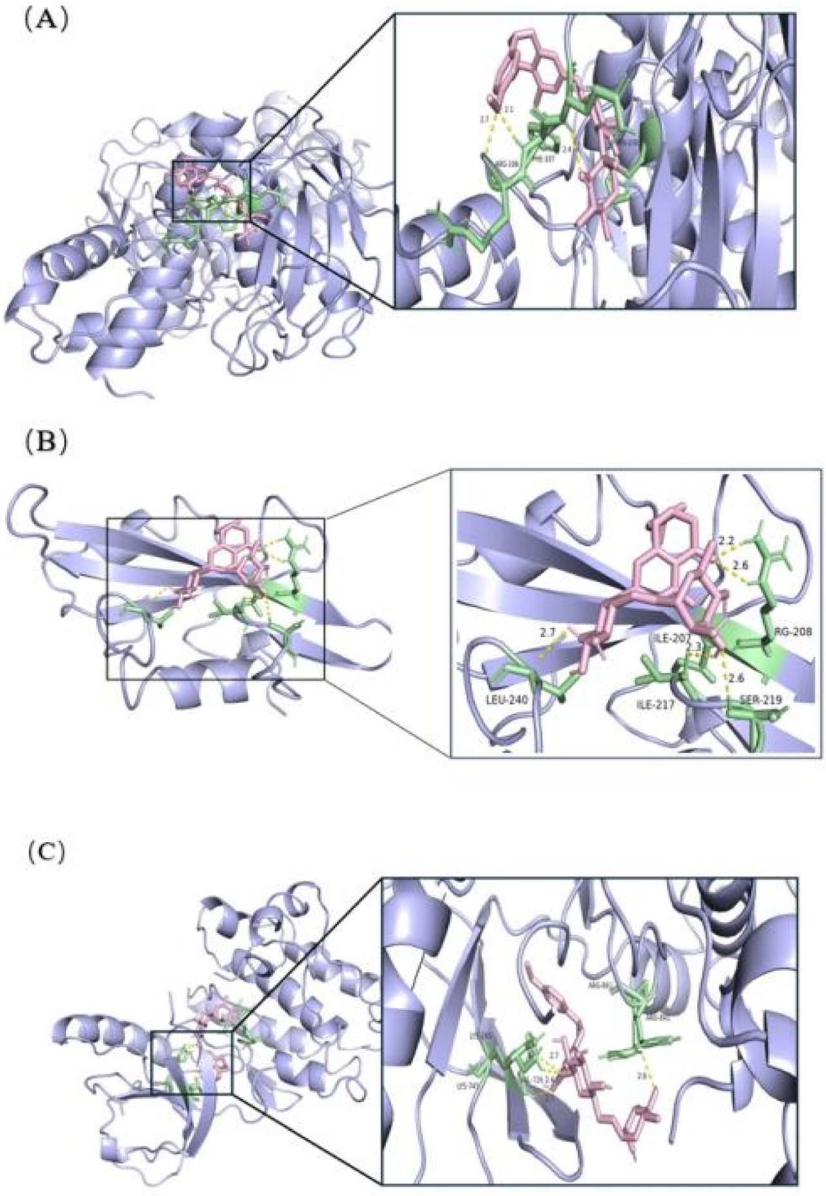

Fig. 5 Visualization of four molecular docking, (A) is MMP9-didymin, (B) is SRC-didymin, (C) is EGFR-didmin.

accounts for approximately 15% of cases and is highly aggressive, characterized by rapid growth, early metastasis, and a five-year survival rate below 5%. In advanced NSCLC, patients often exhibit pulmonary infections and respiratory symptoms such as cough and wheezing, which align with the traditional Chinese medicine (TCM) pattern of lung accumulation.[38] TCM pathogenesis in lung cancer involves deficiency of vital essence and excess of pathogenic factors, warranting treatment strategies that reinforce healthy qi and eliminate pathogenicity.[39] CGT is known to regulate qi, resolve dampness, and eliminate phlegm. However, its specific mechanisms in lung cancer treatment remain unclear. This study applies network pharmacology and molecular docking to explore CGT's potential therapeutic mechanisms.

Using LC-MS, we identified 44 compounds from CGT extracts based on spectral matching (>80% similarity); details are provided in Fig. S2 and Table S5. Bioactive components were screened *via* the TCMSP database using oral bioavailability (OB) ≥30% and drug-likeness (DL) ≥0.18 criteria, yielding 10 active compounds (Table 3). Network analysis highlighted seven key components—5,7,4′-Trimethylapigenin, isosinensetin, sinensetin, nobiletin, didymin, neohesperidin, and naringenin—with node degrees >30, suggesting their central role in CGT's anti-lung cancer effects.

Protein–protein interaction (PPI) analysis of 79 gene targets identified nine core targets: CCND1, PARP1, AKT1, ESR1, EGFR, BCL2, MMP9, SRC, and MTOR. GO enrichment indicated involvement in biological processes such as peptide modification and aging, cellular components including kinase complexes, and molecular functions like tyrosine kinase activity. KEGG analysis linked CGT activity to the EGFR tyrosine kinase inhibitor resistance pathway Fig. S3 for network details and Fig. S4 for enrichment schematics).

Molecular docking between the seven key components and nine core targets showed favorable binding affinities across all pairs.[40] MMP9 exhibited the strongest average binding affinity (-8.6 kcal mol^{-1}), followed by SRC (-8.4 kcal mol^{-1}) and EGFR (-8.2 kcal mol^{-1}), while BCL2 had the weakest (-6.2 kcal mol^{-1}). Among the components, didymin showed the highest average binding affinity (-8.7 kcal mol^{-1}), indicating its potential as the primary anti-lung cancer constituent (Table 4). Docking visualizations of didymin with MMP9, SRC, and EGFR are shown in Fig. 5.

These results are consistent with prior studies reporting that didymin induces apoptosis in lung cancer cells (A549 and NCI–H460) *via* the Fas/FasL pathway and suppresses tumor growth *in vivo*.[41] Didymin also exhibits anti-angiogenic effects by inhibiting VEGF-mediated processes in endothelial cells.[42] Together, this evidence supports didymin as a crucial active component in CGT.

The anti-tumor effects of didymin are likely mediated through its interaction with key signaling molecules that drive cancer progression. Among these,MMP9, a matrix metalloproteinase secreted by various cells, promotes tumor angiogenesis and is overexpressed in pulmonary diseases, correlating with tissue damage and infection severity.[43–45] SRC kinases regulate tumor progression through cytoskeletal dynamics and MMP/VEGF signaling.[46,47] EGFR, a receptor tyrosine kinase, drives proliferation and invasion in cancer and is often dysregulated in lung cancer.[48]

Our GO and KEGG analyses suggest CGT may counteract lung cancer by targeting EGFR tyrosine kinase inhibitor resistance pathways.

In conclusion, didymin is a pivotal active component of CGT against lung cancer, primarily interacting with MMP9, SRC, and EGFR. These findings, consistent with integrated computational analyses, underscore the utility of network pharmacology in uncovering TCM mechanisms and guiding drug discovery. Further experimental validation is needed to confirm this multi-target mechanism.

4. Conclusion

This study developed an efficient and environmentally friendly method for extracting naringin from CGT using a natural deep eutectic solvent (NADES). Among 19 NADES formulations, choline chloride–levulinic acid achieved the highest extraction yield. Optimized conditions (60 °C, 40 min, solid–liquid ratio 1 : 65, 300 W ultrasound) resulted in a naringin yield of 4.7%, outperforming conventional solvents like methanol and ethanol (4%). SEM imaging revealed greater microstructural disruption in NADES-treated samples, supporting its superior efficiency.

Furthermore, network pharmacology and molecular docking analyses identified 10 bioactive compounds and 79 potential therapeutic targets related to lung cancer. These targets are involved in key pathways such as EGFR inhibitor resistance. Strong binding affinities were confirmed between core targets and active compounds suggesting a multi-target mechanism for CGT's anti-lung cancer effects.

Although the proposed NADES method is currently feasible only at the laboratory scale, it offers a sustainable alternative for extracting high-value compounds. Further *in vivo* validation and pharmacokinetic studies are needed to substantiate these findings and support clinical translation.

It should be noted that this study primarily focused on the screening of NADESs and the evaluation of their extraction performance, while the regeneration and recycling of the spent NADES were not investigated. This is undoubtedly a crucial aspect for the industrial application of this technology and will be a key direction for our future research. We will focus on developing efficient and low-cost regeneration methods to improve the overall economic and environmental friendliness of the process.

Conflicts of interest

The authors declare that they no known competing financial interests or personal relationships that could have appeared to influence the work reported in the paper.

Data availability

The data that support the findings of this study are openly available in Science Data Bank at 10.57760/sciencedb.27361.

Supplementary information is available. See DOI: **https://doi.org/10.1039/d5ra07966g**.

Acknowledgements

This work is supported by the sub-project of Research on the Pharmacodynamic Material Basis of Characteristic Chinese Medicinal Materials in Southwest China (2024jbky-027): Mechanism of simultaneous extraction of flavonoids and essential oil components from Fructus aurantii by the "tailored design" NADES based on quantum chemical calculations (No. 2024jbky-kfkt-006).

References

1 L. Wei, Q. Hu, L. He, G. Li, J. Zhang and Y. Chen, *J. Food Sci.*, 2024, **89**, 1454–1472.
2 T. C. Mai, N. T. Tran, D. T. Mai, T. T. Ngoc Mai, N. H. Thuc Duyen, T. N. Minh An, *et al.*, *RSC Adv.*, 2022, **12**, 25962–25976.
3 G. Du, L. Jin, X. Han, Z. Song, H. Zhang and W. Liang, *Cancer Res.*, 2009, **69**, 3205–3212.
4 S. Park, W. Lim, F. W. Bazer and G. Song, *Phytomedicine*, 2018, **50**, 238–246.
5 V. S. Shilpa, R. Shams, K. K. Dash, V. K. Pandey, A. H. Dar, S. Ayaz Mukarram, *et al.*, *Molecules*, 2023, **28**, 5623.
6 X. L. Yu, X. Meng, Y. D. Yan, J. C. Han, J. S. Li, H. Wang, *et al.*, *Molecules*, 2023, **28**, 1939.
7 Y. Shangguan, J. Ni, L. Jiang, Y. Hu, C. He, Y. Ma, *et al.*, *Curr. Res. Food Sci.*, 2023, **7**, 100610.
8 M. Sevindik, A. Gurgen, A. T. Korkmaz and I. Akata, *Molecules*, 2025, **30**, 4006.
9 X. Wang, X. Su, Y. Li, Y. Guan, B. Yan, Y. Liu, *et al.*, *Ultrason. Sonochem.*, 2025, **121**, 107538.
10 T. Yuan, C. Lin, Q. Yu, X. Shi, P. Jin, J. Huang, *et al.*, *Ultrason. Sonochem.*, 2025, **121**, 107545.
11 S. Zhang, Z. Wu, Q. Zhang, H. Zhao and J. Li, *Int. J. Biol. Macromol.*, 2025, **328**, 147484.
12 S. Phaisan, F. Makkliang, W. Putalun, S. Sakamoto and G. Yusakul, *RSC Adv.*, 2021, **11**, 8741–8750.
13 W. Khalid, I. E. Benmebarek, S. Zargarchi, P. Kumar, M. Javed, A. Moreno, *et al.*, *Ultrason. Sonochem.*, 2025, **114**, 107276.
14 H. Li, K. Yang, Y. Yang, L. Ding and X. Li, *Int. J. Pharm.*, 2025, **675**, 125509.
15 Y. J. Liu, L. Lou, Q. Huang, W. Xu and H. Li, *Ultrason. Sonochem.*, 2023, **99**, 106560.
16 Y. C. Wu, P. Wu, Y. B. Li, T. C. Liu, L. Zhang and Y. H. Zhou, *RSC Adv.*, 2018, **8**, 15069–15077.
17 K. Jaikampan, W. Poomanee, T. Thavanapong, C. Chittasupho, K. Jantadee and M. Sainakham, *Plants*, 2025, **14**, 1661.
18 Y. Lou, J. Zhang, X. Wu, J. Li, Q. Zhou, W. Li, *et al.*, *Anal. Methods*, 2025, **17**, 4157–4168.
19 C. Srimawong, P. Torkaew and W. Putalun, *RSC Adv.*, 2025, **15**, 22086–22096.
20 V. Taco, D. Almachi, P. Bonilla, I. Gijon-Arreortua, S. Benali, J. M. Raquez, *et al.*, *Molecules*, 2025, **30**, 3116.
21 P. Sanchez-Arguello and A. Martin-Esteban, *Environ. Res.*, 2025, **263**, 122202.
22 K. Bautista-Rangel, L. F. Losoya-Uribe, M. Rodriguez-Gonzalez, G. Saab-Rincon, A. Lopez-Munguia and E. Castillo, *Int. J. Biol. Macromol.*, 2025, **318**, 145012.
23 Y. Shan, J. Li, Y. Chen, R. Jia, X. Zeng, Y. Li, *et al.*, *J. Chromatogr. B*, 2025, **1263**, 124701.
24 V. M. Tamayo-Rincon, J. Colorado-Rios, D. J. Alvarez-Bustamante, V. Urrea-Victoria, D. M. Marquez-Fernandez, C. H. Salamanca, *et al.*, *Mar. Drugs*, 2025, **23**, 345.
25 M. Wang, S. Fang and X. Liang, *J. Pharm. Biomed. Anal.*, 2018, **158**, 262–268.
26 M. A. Araujo, B. Rodrigues Morais, J. P. da Silva Santos, L. K. de Jesus, K. Aurelio Lomba, G. C. do Nascimento, *et al.*, *Methods Protoc.*, 2025, **8**, 73.
27 D. Caviglia, E. Russo, A. M. Schito, F. S. Robustelli Della Cuna, E. Grignani, N. Lionetti, *et al.*, *Molecules*, 2025, **30**, 3549.
28 F. Limongelli, A. M. Aresta, R. Tardugno, M. L. Clodoveo, A. Barbarossa, A. Carocci, *et al.*, *Molecules*, 2025, **30**, 4090.
29 M. Martinovic, I. Nesic, A. Zugic and V. M. Tadic, *Plants*, 2025, **14**, 2738.
30 X. Yu, X. Meng, Y. Yan, H. Wang and L. Zhang, *Molecules*, 2022, **27**, 9026.
31 S. Wang, Z. Qin, Y. Wang, L. Liu and Z. Tan, *Foods*, 2022, **11**, 2566.
32 A. Kowaluk, J. Guedon, N. Kryska, D. Rabiej-Koziol, M. Strzelec and A. Szydlowska-Czerniak, *Foods*, 2025, **14**, 3172.
33 E. Truzzi, D. Bertelli, B. Catellani, D. D. Jazi and S. Benvenuti, *Molecules*, 2025, **30**, 1164.
34 Q. Yu, M. Yang, L. Yang, M. Li and Y. Yang, *Molecules*, 2024, **29**, 3738.
35 M. Raza, A. Husain, M. Jawaid, A. Inayat, Y. E. Greish, A. Meraj, *et al.*, *Int. J. Biol. Macromol.*, 2025, **321**, 146497.
36 T. Sebbah, I. Yahla, E. Cunha, A. Riazi, C. G. Amorim, J. M. Rodriguez-Diaz, *et al.*, *Antioxidants*, 2025, **14**, 239.
37 K. Shanmugapriya and H. W. Kang, *Int. J. Biol. Macromol.*, 2025, **321**, 146591.
38 C. R. Pendkar, *Cureus*, 2025, **17**, e90957.
39 Y. Wang, C. Wang, G. Zhao, J. Ding, Y. Cai, P. Ma, *et al.*, *Pharmacol. Res.*, 2024, **208**, 107371.
40 S. Chang, S. Wen, W. Zhang, H. Zhang, Y. Guo, Q. Wang, *et al.*, *Front. Med.*, 2025, **12**, 1573241.
41 J. Y. Hung, Y. L. Hsu, Y. C. Ko, Y. M. Tsai, C. J. Yang, M. S. Huang, *et al.*, *Lung Cancer*, 2010, **68**, 366–374.
42 K. Shukla, H. Sonowal, A. Saxena and K. V. Ramana, *Vasc. Pharmacol.*, 2019, **115**, 18–25.
43 K. Augoff, A. Hryniewicz-Jankowska, R. Tabola and K. Stach, *Cancers*, 2022, **14**, 1849.
44 Y. K. Choi, J. I. Kang, D. H. Yang, S. C. Han, K. J. Kim, H. J. Boo, *et al.*, *In Vivo*, 2025, **39**, 2035–2049.
45 H. Zhang, Z. Wang, J. Li, Y. Jia, X. Xie, Y. Ding, *et al.*, *Int. Immunopharmacol.*, 2025, **162**, 115109.
46 M. D. Brada, T. Karakulak, P. Schraml, M. Haberecker, D. Rutishauser, J. S. Ross, *et al.*, *J. Pathol.:Clin. Res.*, 2025, **11**, e70028.
47 A. Li and R. Wang, *Bull. Exp. Biol. Med.*, 2025, **178**, 460–466.
48 Y. Sakata, G. Saito, S. Sakata, T. Yamaguchi, M. Tamiya, H. Suzuki, *et al.*, *Clin. Lung Cancer*, 2025, **26**, e328–e335.